

LIGHT CURVE AND SPECTRAL MODELS FOR THE HYPERNOVA SN 1998BW ASSOCIATED WITH GRB980425

TAKAYOSHI NAKAMURA¹, PAOLO A. MAZZALI^{2,5}, KEN'ICHI NOMOTO^{3,5}, KOICHI IWAMOTO⁴*Submitted to the Astrophysical Journal on 28 June 2000*

ABSTRACT

A refined model for the unusual Type Ic supernova 1998bw, discovered as the optical counterpart of GRB980425, is presented, and synthetic light curves and spectra are compared with the observations. The first 30 days of the light curve and the broad line features of the spectra can be reproduced with the hydrodynamical model of the explosion of a $14M_{\odot}$ C+O star, the core of a star with initial mass $40M_{\odot}$, assuming that the explosion was very energetic (kinetic energy $E_K = 5 \times 10^{52}$ erg) and that $0.4M_{\odot}$ of ^{56}Ni were synthesized. At late times, however, the observed light curve tail declines more slowly than this energetic model, and is in better agreement with a less energetic ($E_K = 7 \times 10^{51}$ erg) one. This shift to a less energetic model may imply that the inner part of the ejecta has higher density and lower velocities than the spherically symmetric model with $E_K = 5 \times 10^{52}$ erg, so that γ -rays deposit more efficiently. We suggest that an aspherical explosion can produce such a structure of the ejecta. We also study detailed nucleosynthesis calculations for hyper-energetic supernova explosions and compare the yields with those of normal supernovae.

Subject headings: gamma-ray burst — supernovae — supernovae: individual (SN1998bw) — nucleosynthesis

1. INTRODUCTION

On 1998 April 25, GRB980425 triggered the Narrow Field Instrument (NFI) and Wide Field Camera (WFC) detectors on board *BeppoSAX* (Soffitta et al. 1998). SN 1998bw was discovered within the WFC error box in the optical (Galama et al. 1998a) and radio wavelength bands (Kulkarni et al. 1998a) only 0.9 and 3 days after the date of the GRB, respectively. The X-ray afterglow detected by the NFI within the error box of GRB980425 is consistent with SN 1998bw (Pian et al. 1999). The small likelihood of finding a supernova and a GRB in such a small field over such a short interval of time suggests that SN 1998bw and GRB980425 are related (Galama et al. 1998b; Kulkarni et al. 1998b).

The early optical spectra of SN 1998bw apparently lack dominant line features, displaying only some broad emissions at 500, 620 and 800 nm (Galama et al. 1998b; Stathakis et al. 2000; Patat et al. 2000). These were shown to be the emission components of P-Cygni profiles of very broad line blends. They are caused mostly by FeII lines in the blue, by SiII near 600 nm and by OI + CaII near 720 nm (Iwamoto et al. 1998, hereafter IMN98). The absence of any hydrogen line after subtraction of the galaxy background and the fact that the Si II line at 615 nm has a very large velocity indicate that the supernova is neither a Type II nor a normal Type Ia (Galama et al. 1998b). Following the conventional classification scheme (Filippenko 1997), the lack of strong He I features led Patat & Piemonte (1998) to conclude that SN 1998bw is likely to be a Type Ic supernova (SN Ic) rather than a Type Ib.

The light curve of SN 1998bw (Galama et al. 1998b) showed a very early rise and reached a peak at ~ 17 days (in the V band) after the explosion, and then has been declining exponentially with time (McKenzie & Schaefer 1999; Patat et al. 2000). This clearly indicates that the light curve is not a typical optical afterglow of a gamma-ray burst, but it is powered by the radioactive decay of ^{56}Ni and ^{56}Co as in usual supernovae (IMN98). The distance modulus to SN 1998bw is estimated as $\mu = 32.89$ mag, so that the peak luminosity of SN 1998bw is $\sim 1 \times 10^{43}$ ergs sec $^{-1}$, which is about ten times brighter than typical SNe Ib/Ic (Clocchiatti & Wheeler 1997). To achieve such a high luminosity, a large amount of ^{56}Ni must have been synthesized in SN1998bw (IMN98; Woosley, Eastman & Schmidt 1999), again about ten times as much as that produced in typical core-collapse-induced supernovae. The very broad spectral features and the light curve shape led various groups to the conclusion that SN 1998bw had a very large kinetic energy of explosion E_K (IMN98; Woosley et al. 1999; Branch 2000).

IMN98 constructed models of the core-collapse-induced explosion of C+O cores of initially massive stars that had lost their hydrogen and helium-rich layers before the explosion. Among those models, the energetic explosion ($E_K \sim (2 - 5) \times 10^{52}$ ergs) of a C+O star of $13.8 M_{\odot}$ successfully fit the first 60 days of the light curve and the early spectra, although the synthetic spectral lines were still narrower than the very broad observed features (IMN98). Since the kinetic energy is more than one order of magnitude larger than the energy of typical supernovae, SN 1998bw was called a “hypernova” (IMN98), a term we

¹Department of Astronomy, School of Science, University of Tokyo, Tokyo, Japan; nakamura@astron.s.u-tokyo.ac.jp²Osservatorio Astronomico di Trieste, Trieste, Italy; mazzali@ts.astro.it³Department of Astronomy, School of Science, University of Tokyo, Tokyo, Japan; nomoto@astron.s.u-tokyo.ac.jp⁴Department of Physics, College of Science and Technology, Nihon University, Tokyo, Japan; iwamoto@etoile.phys.cst.nihon-u.ac.jp⁵Research Center for the Early Universe, School of Science, University of Tokyo, Tokyo, Japan

use to describe events with $E_K \gtrsim 10^{52}$ erg without specifying whether the central engine is a collapsar (MacFadyen & Woosley 1999), a magnetar (Nakamura 1998; Wheeler et al. 2000) or a pair-instability supernova (Heger et al. 2000; Nakatsuru et al. 2000).

Interestingly, photometry after ~ 60 days showed that SN 1998bw declined significantly more slowly than the rate predicted by the model of IMN98 (McKenzie & Schaefer 1999; Patat et al. 2000). Also the bolometric light curve has been constructed up to day 500 (Patat et al. 2000). Therefore, we have recomputed the light curve of SN 1998bw using progenitors of different masses and explosions of different energies, and provide better estimates for these parameters.

The hydrodynamical models for SN 1998bw are described in §2. Sections 3 and 4 are devoted to light curve models and synthetic spectra models, respectively. Explosive nucleosynthesis in SN 1998bw is discussed in §5. Finally, the nature of this peculiar supernova is summarized in §6, with the emphasis being placed on possible evidence that the explosion was aspherical. Preliminary results have already been reported by Nakamura et al. (1999a, 2000) and Nomoto et al. (2000ab).

2. HYDRODYNAMICAL MODELS FOR SN 1998BW

Hydrodynamical models are constructed as follows. C+O stars are chosen as progenitors as in IMN98. Light curves and spectra are computed for various C+O star models with different values of the kinetic energy E_K and the ejecta mass M_{ej} . These parameters can be constrained by comparing calculated light curves, synthetic spectra, and photospheric velocities with the observational data of SN 1998bw.

- (1) In the ordinary, low energy SN Ic model (model CO138E1), a C+O star with a mass $M_{CO} = 13M_\odot$ (which is the core of a $40M_\odot$ main-sequence star; Nomoto & Hashimoto 1988; Nomoto et al. 1997) explodes with $E_K = 1.0 \times 10^{51}$ ergs and $M_{ej} = M_{CO} - M_{cut} \simeq 12M_\odot$. M_{cut} ($= 2M_\odot$ in this case) denotes the position of the mass cut, which corresponds to the mass of the compact star remnant. This is either a neutron star or a black hole, depending on M_{cut} .
- (2) For the hypernova models CO138E50, CO138E30, and CO138E7, the progenitor C+O star of $M_{CO} = 13.8M_\odot$ is the same as in CO138E1. These models have different explosion energies: $E_K = 5 \times 10^{52}$ erg (CO138E50), 3×10^{52} erg (CO138E30), and 7×10^{51} erg (CO138E7). The ejecta mass is $M_{ej} \simeq 10 - 11.5M_\odot$, i.e., $M_{cut} \simeq 2.5 - 4M_\odot$. The parameters of the models are summarized in Table 1. The position of the mass cut is chosen so that the ejected mass of ^{56}Ni is the value required to explain the observed peak brightness of SN 1998bw by radioactive decay heating. The compact remnant in these hypernova models may well be a black hole, because M_{cut} can exceed, sometimes significantly, the maximum mass of a stable neutron star.

The hydrodynamics at early phases was calculated using a Lagrangian PPM code (Colella & Woodward 1984). All

models are spherically symmetric. The explosion is triggered by depositing thermal energy in a couple of zones just below the mass cut so that the final kinetic energy has the required value. A strong shock wave forms and propagates toward the surface. Explosive nucleosynthesis takes place behind the shock wave. Radioactive ^{56}Ni is produced in the deep, low velocity layers of the ejecta.

In SN II and SN Ib models, it has been demonstrated that Rayleigh-Taylor instabilities develop at the H/He and He/C+O interfaces and induce mixing of elements in the ejecta (e.g., Arnett et al. 1989; Hachisu et al. 1991; Iwamoto et al. 1993). Bare C+O stars, the progenitors of SNe Ic, lack composition interfaces with such pronounced density jumps. However, polarization measurements suggested that SNe Ic, and hypernovae in particular, are asymmetric explosions (Wang et al. 1999; Danziger et al. 1999; Patat et al. 2000). The asymmetry of the explosion may strengthen the instability and bring heavy elements up to high velocity layers. This is particularly true of jet-like explosions, where it is likely that extensive mixing takes place in velocity space. In view of the large uncertainties in our knowledge of the mixing process, we assume that the material ejected is uniformly mixed out to a velocity $v = v_{\text{mix}}$.

The hydrodynamical models become homologous ($v \propto r$) at $t \sim 250$ sec, and are then used as input for a radiation transfer code. The lines in Figure 1 show the density-velocity distribution of the homologously expanding ejecta (top) and the enclosed mass M_r as a function of velocity (bottom) for models CO138E50 (solid), CO138E30 (long-dashed), CO138E7 (short-dashed), and CO138E1 (dash-dotted).

3. LIGHT CURVE MODELS

Synthetic light curves are computed with a radiative transfer code (Iwamoto et al. 2000) which takes into account the balance between photo-ionizations and recombinations and includes a simplified treatment of line opacity. The width of the light curve peak, τ_{LC} , depends on E_K and M_{ej} approximately as $\tau_{LC} \sim (\kappa/c)^{1/2} M_{ej}^{3/4} E_K^{-1/4}$, where κ and c are the optical opacity and the speed of light, respectively (Arnett 1982). This means that the light curve can be reproduced with different explosion models that have the same values of M_{ej}^3/E_K . However, these parameters can be further constrained from both photospheric velocities and spectra because the velocity scales roughly as $M_{ej}^{-1/2} E_K^{1/2}$. The light curve shape depends also on the distribution of the radioactive heating source ^{56}Ni , for which we examine the dependence on v_{mix} (§2).

Our calculations are compared with the bolometric light curve of SN 1998bw constructed by Patat et al. (2000), which uses a redshift distance $\mu = 32.89$ mag ($d = 37.8$ Mpc, $H_0 = 65 \text{ km s}^{-1} \text{ Mpc}^{-1}$) and $A_V = 0.05$ mag. The time of core collapse is set at the detection of GRB 980425. Figure 2 shows the bolometric light curves of the energetic models CO138E50 (solid) and CO138E30 (long-dashed), and Figure 3 the less energetic models CO138E7 (short-dashed) and CO138E1 (dash-dotted).

Figure 4 shows the evolution of the calculated photospheric velocities of CO138E50 (solid line), CO138E30 (long-dashed line), CO138E7 (short-dashed line), and CO138E1 (dash-dotted line) compared with those ob-

tained from spectral models (filled circles), the observed velocities of the Si II 634.7, 637.1 nm lines measured in the spectra at the absorption core (open circles; Patat et al. 2000), and that of the Ca II H + K doublet measured in the spectrum of May 23 (square; Patat & Piemonte 1998).

3.1. Early Phase

The early part of the light curve ($t \lesssim 25$ days) is well reproduced by the two energetic models, CO138E50 and CO138E30. The difference between the two curves is too small to see on the scale of Figure 2 because the light curve width scales as $E_K^{-1/4}$. The early part of the light curve also depends on the ^{56}Ni distribution in the ejecta. To reproduce the early sharp rise of the light curve, extensive mixing of ^{56}Ni , out to $v_{\text{mix}} = 22,000 \text{ km s}^{-1}$ for CO138E50 and $v_{\text{mix}} = 30,000 \text{ km s}^{-1}$ for CO138E30, is required. A better fit can be obtained, if we adopt the following ad hoc ^{56}Ni distribution: $X(^{56}\text{Ni}) = 0.79$ at $v \leq 11,000 \text{ km s}^{-1}$, 0.011 at $v = 11 - 17,000 \text{ km s}^{-1}$, and 0.032 at $v = 17 - 40,000 \text{ km s}^{-1}$, where $X(^{56}\text{Ni})$ denotes the mass fraction of ^{56}Ni . The result is shown in Figure 5. Such a non-uniform distribution of ^{56}Ni might reflect a complicated structure of a possible jet-like ejecta. The ^{56}Ni mass is determined to be $0.4 M_{\odot}$ from the fitting of the maximum luminosity and the date of maximum. (Note that IMN98 slightly overestimated the mass of ^{56}Ni because they assumed the negligible bolometric correction and adopted a different absorption and distance.)

In contrast, the early light curves of the less energetic models (CO138E7 and CO138E1) evolve too slowly, reaching the maximum too late as compared with the observations (Figure 3), even if ^{56}Ni is distributed uniformly throughout the ejecta.

The photospheric velocities v_{ph} provide clearer diagnostics to distinguish between CO138E50 and CO138E30. In the early phase ($t < 20$ days), v_{ph} of CO138E50 is in good agreement with the observed v_{ph} , while v_{ph} of CO138E30 is clearly too low to be consistent with the observations (Fig. 4).

As far as the early phase ($t < 20$ days) is concerned, CO138E50 shows the best agreement with both the light curve and photospheric velocities of SN 1998bw. The synthetic spectra also require the most energetic model CO138E50 as will be shown in §4. CO138E50 has the same mass as the best model in IMN98 but has a larger E_K , which is necessary especially to improve the fit to the spectra (§4).

3.2. Intermediate Phase

At late phases, the decline rate of the light curve is determined mainly by the fraction of the gamma-rays emitted by the ^{56}Co decay which is trapped in the ejecta. The optical depth of the ejecta to the gamma-rays scales as $\kappa_{\gamma}\rho R \propto MR^{-2} \propto M^2 E_K^{-1} t^{-2}$. Thus the model dependence can be seen more easily than at earlier phases as follows:

- (1) The light curve of CO138E50 is consistent with SN1998bw until day 50 but declines faster than the observation afterwards (Figure 2; McKenzie & Schaefer 1999; Patat et al. 2000). The light curve of CO138E30 declines more slowly than that

of CO138E50, and is in better agreement with SN1998bw, but it still declines faster than the observations.

- (2) The photospheric velocity v_{ph} shows a similar tendency. Figure 4 shows that v_{ph} of CO138E50 declines much faster than the observations, because the photosphere recedes inwards in mass too rapidly. On the other hand, v_{ph} of CO138E30 fits the observations better than CO138E50 after day 20.
- (3) Figure 3 shows that the apparently exponential decline of SN1998bw after day 60 (McKenzie & Schaefer 1999; Patat et al. 2000) is well reproduced by the lower energy model CO138E7, where trapping is more efficient, but the low flux level requires a reduced ^{56}Ni mass of $0.28 M_{\odot}$ (dotted line). Note, however, that $0.28 M_{\odot}$ of ^{56}Ni is too small to reproduce the observed light curve maximum.
- (4) The normal SN Ic model CO138E1 in Figure 3 is slow enough to trap most of the gamma-rays emitted from the ^{56}Co decay. Then the decline of its light curve is too slow compared with the observed rate.

These comparisons between SN 1998bw and the model light curves and v_{ph} in Figures 2, 3, & 4 indicate that:

- (i) The explosion seems to be as energetic as CO138E50 at early phases, when the expansion velocities in the outer layers are as fast as those of CO138E50 as also indicated from the spectral evolution (§4).
- (ii) γ -ray deposition at later phases is more efficient than predicted by the most energetic models. This can be realized if there exists a significant amount of low-velocity and/or high-density material containing ^{56}Ni or simply trapping the γ -rays. In this case a larger fraction of γ -rays would be trapped and the light curve would decline as slowly as CO138E7.

Indications of the presence of a low-velocity, high-density region are also found for SN 1997ef (Iwamoto et al. 2000; Mazzali et al. 2000a), a lower-energy analogue of SN 1998bw. This fact suggests a departure of the ejecta structure from spherical symmetry. We will discuss this point further in §6 in combination with the spectra. In any case, some modifications of the spherical hydrodynamical models appear to be necessary.

3.3. Late Phase

After day ~ 200 the decline of the model light curve becomes slower, and it approaches the half-life of ^{56}Co decay around day 400. At $t \gtrsim 400$ days most γ -rays escape from the ejecta. The γ -ray deposition fraction at 400 days is 1%, 1.5%, 6%, and 13% for CO138E50, E30, E7, and E1, respectively. On the other hand, positrons emitted from the decay of ^{56}Co are supposed to be fully thermalized because of the postulated weak magnetic field (e.g., Colgate & Petrich 1979). Therefore, positron deposition determines the light curve at $t \gtrsim 400$ days (dotted line in Figure 2). If the observed tail should follow the positron-powered light curve, the ^{56}Co mass could be determined directly. Since positron deposition should occur almost on

the spot, this determination does not depend much on any asphericity of the ejecta.

Recently ($t = 778$ days), HST has observed a source at the position of SN1998bw/GRB980425 (Holland et al. 2000). Although the source is somewhat extended, the detection magnitude (AB magnitudes of 26.2 ± 0.1 in the STIS clear filter and 26.3 ± 0.1 in the STIS long pass filter) is consistent with the prediction of model CO138E50.

4. SYNTHETIC SPECTRA

In Figure 6 we show the synthetic spectra obtained for the same 3 epochs fitted in IMN98 (continuous lines) compared with spectra observed at ESO (bold lines). We used model CO138E50 and computed synthetic spectra with a Monte Carlo model (Mazzali & Lucy 1993), improved with the inclusion of photon branching and a new extended and improved line list (Lucy 1999; Mazzali 2000). The synthetic spectra are computed using the luminosity derived from the light curve, a distance modulus of $\mu = 32.89$ mag and $A_V = 0.05$. The assumption of very small reddening is supported by the upper limit of 0.1 Å in the equivalent width of the Na I D line obtained from high-resolution spectra (Patat et al. 2000). The observed spectra used here (solid lines) are the ‘definitive’, fully reduced version of the same ESO spectra shown in IMN98, and are calibrated with respect to the V photometry. The residual correction factors for the other bands are usually very close to 1, but they are ~ 1.1 for B in the May 11 and 23 spectra. Therefore, the new models (i.e., 3 epochs of CO138E50) have somewhat different parameters than those of IMN98. Both the luminosities and the photospheric velocities are larger than IMN98. The photospheric velocity is now in better agreement with the measured velocity of the Si II line than in Figure 3 of IMN98.

The synthetic spectra clearly improve over those of IMN98, especially at the earliest epochs. Absorptions not caused by broad blends of many lines of moderate strength, such as the Si II feature near 6000Å and, in particular, the O I+Ca II feature between 7000 and 8000Å, are now much broader, in significantly better agreement with the data. Nevertheless, the blue sides of those absorptions are still too narrow, indicating that even the new model CO138E50 may not contain enough mass at the highest velocities.

Therefore we introduced an arbitrary change to the original CO138E50 density structure. Several possibilities were tested, and satisfactory results were found when the density slope was reduced from $\rho \propto r^{-8}$ to $\rho \propto r^{-6}$ at $v > 30,000$ km s $^{-1}$. This does not introduce a significant change in M_{ej} , and increases E_K by only about 10%, but it does increase the density at high velocities, leading to significant absorption at $v \sim 60,000$ km s $^{-1}$ in the strongest lines, especially the Ca II IR triplet, extending the absorption troughs to the blue. The corresponding synthetic spectra are shown as the dotted lines in Figure 6. The effect of the change is of course largest at the earliest epochs. The overall agreement with the observed spectra is better, although several problems remain, the most severe of which is clearly the excessive strength of the O I line at 7200Å on May 11 and 23. The composition is dominated by O, and it is difficult to make that line become weaker. On 23 May, the synthetic Ca II IR triplet matches the weak feature at 8000Å, which is first seen on 11 May and which continues to grow until it finally causes the wavelength

of the absorption minimum of the entire broad feature to shift to ~ 8200 Å (Patat et al. 2000). This is rather a peculiar behavior, because on 3 May the O I and Ca II lines had to blend much more to give rise to the observed broad feature, which then had a minimum at 7000Å. The synthetic O I line is too strong and too fast. The core of the broad feature, if it is interpreted as O I 7774Å, indicates a velocity of 10500 km s $^{-1}$ on May 11 and 6000 km s $^{-1}$ on May 23. This is significantly lower than the corresponding velocity of the model photosphere. Actually, the definition of a photosphere at very red wavelengths is not very accurate, because the density of spectral lines is low and so line opacity does not define a pseudo-continuum in that region. Therefore, the observations probably indicate that a large fraction of the O is located at low velocities.

A very flat ($\rho \propto r^{-2}$) density distribution was also used by Branch (2000) to fit the spectrum of SN 1998bw. This dependence is however too flat when we use our MC model, because the ionization of, e.g., Ca II does not fall as steeply as he assumed. On the other hand, Branch’s value of E_K (5×10^{52} erg) is similar to ours, but he quotes a mass of $6M_\odot$ above 7000 km s $^{-1}$, while in our case the mass above that velocity is as large as $\sim 10M_\odot$. Such a flat density distribution at high velocities is also required to fit the spectrum of another hypernova SN1997ef (Mazzali et al. 2000a). This might indicate that progenitors of these hypernovae underwent very extensive mass loss; the outer density structure of the ejecta is flatter than that of ordinary giants.

Clearly, a definitive solution has not been found yet. It is quite possible that only by taking into account departures from spherical symmetry it will be possible to obtain a really accurate fit to the spectra. Nevertheless, considering the complexity of the problem, our synthetic spectra at least demonstrate that a large E_K is necessary and that the O-dominated composition of the SN Ic model yields quite a reasonable reproduction of the observations.

5. EXPLOSIVE NUCLEOSYNTHESIS

We calculated explosive nucleosynthesis using a detailed nuclear reaction network (Thielemann, Nomoto & Hashimoto 1996; Nakamura et al. 1999b). Our calculations are performed in two steps. The first step is a hydrodynamical simulation of the explosions with a small nuclear reaction network which contains only 13 alpha nuclei (^4He , ^{12}C , ^{16}O , ^{20}Ne , ^{24}Mg , ^{28}Si , ^{32}S , ^{36}Ar , ^{40}Ca , ^{44}Ti , ^{48}Cr , ^{52}Fe , and ^{56}Ni) as described in §2. In the second step, at each mesh point of the hydrodynamical model, post-processing calculations are performed with the extended reaction network (Hix & Thielemann 1996), which contains 211 isotopes up to ^{71}Ge .

The top panel of Figure 7 shows the isotopic composition of the ejecta of the hypernova model CO138E50 as a function of the enclosed mass M_r and of the expansion velocity. The nucleosynthesis in other hypernova and supernova models (CO138E30, CO138E7, CO138E1) is also shown in Figure 7 for comparison. The yields of the hypernova and supernova models are summarized in Table 2. Table 3 and Figure 8 give respectively more detailed yields and the abundances of stable isotopes relative to the solar values for model CO138E50. From these figures and tables, we note the following characteristics of nucleosynthesis of hyper-energetic explosions compared with normal

energy explosions.

- (1) The complete Si-burning region where ^{56}Ni is produced is extended further out (in mass coordinates) as the explosion energy increases. How much processed matter is ejected from this region depends on the mass cut. Compared with normal core-collapse supernovae, the much larger amount of ^{56}Ni ($\sim 0.4M_{\odot}$) observed in SN1998bw implies that the mass cut is deeper, so that the elements synthesized in this region, such as ^{59}Cu , ^{63}Zn , and ^{64}Ge (which decay into ^{59}Co , ^{63}Cu , and ^{64}Zn , respectively), are ejected more abundantly. Among hypernova models, more energetic models produce more ^{56}Ni in the incomplete Si burning region (See (3) below), and thus M_{cut} is larger to eject $\sim 0.4M_{\odot}$ ^{56}Ni as constrained from the light curve of SN 1998bw (Figure 7).
- (2) In the complete Si-burning region of the hypernova models (CO138E50/E30), elements produced by α -rich freezeout are enhanced because nucleosynthesis proceeds at lower densities than in CO138E1. Figure 7 clearly shows a trend that a larger amount of ^4He is left in more energetic explosions. Hence, the mass fractions of the species synthesized through α -particle capture, such as ^{44}Ti and ^{48}Cr (which decay into ^{44}Ca and ^{48}Ti , respectively) are larger in CO138E50/E30/E7 than CO138E1. The integrated mass of these species depend on M_{cut} . For CO138E50, the ejected mass of ^{44}Ti is smaller than in other models because of its larger M_{cut} . Note that the ^4He produced even in the most energetic models has a velocity significantly smaller than that of the He shell identified in SN 1998bw at a velocity of 18300 km s^{-1} by Patat et al. (2000) on the basis of near-IR spectra. Spectral evidence for low velocity He in SN 1998bw is unclear, however the distribution of He depends on mixing in velocity space.
- (3) The incomplete Si-burning region is more massive in more energetic explosions. The main products in this region are ^{28}Si , ^{32}S , and ^{56}Ni . CO138E50 produces $0.2M_{\odot}$ of ^{56}Ni in this region. Other important species such as ^{52}Fe , ^{55}Co , and ^{51}Mn (decaying into ^{52}Cr , ^{55}Mn , and ^{51}V , respectively) are synthesized more abundantly in the more energetic explosions.
- (4) For the larger explosion energy, oxygen burning takes place in more extended, lower density regions. O, C, and Al are burned more efficiently in these cases, and the abundances of the elements in the ejecta are smaller, while a larger amount of ash products such as Si, S and Ar is synthesized by oxygen burning.

6. CONCLUSIONS AND DISCUSSION

In this paper, we presented a model for SN 1998bw which is in better agreement with the early observations than the previous model in IMN98. Models with different E_{K} yield different synthetic spectra, and by comparing with the observed early-time spectra of SN 1998bw and trying to fit the very broad absorption features, we selected model CO138E50 with $M_{\text{ej}} = 10M_{\odot}$ and $E_{\text{K}} = 5 \times 10^{52}$ erg as the best match to the early data. The large value of E_{K} qualifies SN 1998bw as ‘the’ Type Ic Hypernova. (SN IIn

1997cy may be called a “Type IIn Hypernova”; Germany et al. 2000.; Turatto et al. 2000). The mass of the progenitor C+O star is $13.8M_{\odot}$, corresponding to a main sequence mass of $\sim 40M_{\odot}$. All models require $M(^{56}\text{Ni}) \sim 0.4M_{\odot}$ to power the bright light curve peak. This is about an order of magnitude larger than in typical core-collapse SNe. The compact remnant is likely a black hole, because its mass exceeds $\sim 3M_{\odot}$ as constrained from the mass of ^{56}Ni .

Although the early light curve of SN1998bw ($t \lesssim 50$ days) is reproduced well by the most energetic model CO138E50, the observed tail declines more slowly than this model does (§3). The lower energy model CO138E30 is in better agreement with observations at $t \lesssim 100$ days but it still declines too fast. This suggests that there might be a high density region with low velocities in SN1998bw where the γ -rays deposit efficiently, compared with the spherical model CO138E50 (Figure 1). The observations might also be explained if the density structure of the ejecta is assumed to be somewhat aspherical, a possibility which is also supported by the observed polarization ($\sim 0.5\%$) of the early optical light (Patat et al. 2000; IMN98). Model CO138E7 has a slower tail and can reproduce the observed light curve tail if a lower ^{56}Ni mass of $0.28 M_{\odot}$ is adopted.

If the outburst in SN1998bw took the form of a prolate spheroid, for example, the explosive shock was probably strong along the long axis, ejecting material with large velocities and producing abundant ^{56}Ni , which might have caused the early bright light curve. In directions away from the long axis, on the other hand, oxygen would not be consumed, and the density could be high enough for γ -rays to be trapped even at advanced phases, thus giving rise to the slowly declining tail. These features can be seen in the hydrodynamical models of jet-like explosions (MacFadyen & Woosley 1999; Khoklov et al. 1999; Maeda et al. 2000; Nagataki et al. 1997). The fact that the late light curve is fitted by model CO138E7 with $0.28 M_{\odot}$ of ^{56}Ni , while the early light curve requires as much as $0.4 M_{\odot}$, could also support this suggestion, and point at the geometrical ratio between the extension of the high- and low-density regions.

The possible connection between SN 1998bw and GRB980425 also supports the conjecture that SN 1998bw was aspherical. The energy of photons produced by synchrotron emission at the relativistic shock is approximately given by $h\nu \sim 160 \text{ keV} (\Gamma/100)^4 n_1^{1/2}$ (Piran 1999), where Γ is the Lorentz factor of the shock and n_1 (cm^{-3}) is the density of the interstellar matter. In order to produce an observable GRB, Γ should be as large as $\Gamma \sim 100$. However, even the most energetic model (CO138E50) only has a very small mass of relativistic ejecta ($\sim 10^{-10} M_{\odot}$ with $\Gamma \geq 100$). Such a small amount of relativistic material, which is consistent with previous works (IMN98, Woosley et al. 1999), is not enough to produce GRB980425 in a spherically symmetric model. However, if the explosion is axi-symmetric, for instance, the energy can be carried by only a small fraction of the material, which might reach a large enough Lorentz factor.

Regarding asphericity, we note that Danziger et al. (1999) and Mazzali et al. (2000b; see also Nomoto et al. 2000a) estimated a ^{56}Ni mass of $0.35 - 0.65 M_{\odot}$ from the nebula lines of Fe of SN 1998bw. This estimate does not

depend much on the asphericity, and is in good agreement with the ^{56}Ni mass of the spherical models CO138. On the other hand, Höflich et al. (1999) suggested that the ^{56}Ni mass can be as small as $0.2 M_{\odot}$ if aspherical effects are large. These results suggest that the aspherical effects might be modest in SN 1998bw. If we can determine the ^{56}Ni mass more accurately from the late observations, it would provide a good measure of the degree of the as-

phericity.

We would like to thank Ferdinando Patat and Enrico Cappellaro for useful information and discussion on the observations of SN1998bw. This work has been supported by the grant-in-Aid for Scientific Research (12640233, 12740122) and COE research (07CE2002) of the Japanese Ministry of Education, Science, Culture, and Sports.

REFERENCES

Arnett, W.D. 1982, A&A, 253, 785
 Arnett, W.D., Fryxell, B., & Mueller, E. 1989, ApJ, 341, 63
 Branch, D. 2000, in Supernovae and Gamma Ray Bursts, ed. M. Livio et al. (Cambridge: Cambridge University Press), in press
 Baron, E., Young, T. R., & Branch, D. 1993, 409, 417
 Clocchiatti, A., & Wheeler, J. C. 1997, ApJ, 491, 375
 Colella, P., & Woodward, P. R. 1984, J. Comput. Phys. 54, 174
 Colgate, S. A., & Petschek, A. G. 1979, ApJ, 229, 682
 Danziger, I. J., et al. 1999, in The Largest Explosions Since the Big Bang: Supernovae and Gamma Ray Burst, eds. M. Livio, et al. (Baltimore: STScI), 9
 Filippenko, A. V. 1997, Annu. Rev. Astron. Astrophys., 35, 309
 Galama, T. J., Vreeswijk, P. E., Frontera, F., Doublier, V., & Gonzalez, J. F. 1998a, IAU Circ. No. 6895
 Galama, T. J., Vreeswijk, P. M., Van Paradijs, J., Kouveliotou, C., Augusteijn, T., Bohnhardt, H., Brewer, J. P., Doublier, V., Gonzalez, J.-F., Leibundgut, B., Lidman, C., Hainaut, O. R., Patat, F., Heise, J., in't Zand, J., Hurley, K., Groot, P. J., Strom, R. G., Mazzali, P. A., Iwamoto, K., Nomoto, K., Umeda, H., Nakamura, T., Young, T.R., Suzuki, T., Shigeyama, T., Koshut, T., Kippen, M., Robinson, C., de Wildt, P., Wijers, R. A. M. J., Tanvir, N., Greiner, J., Pian, E., Palazzi, E., Frontera, F., Masetti, N., Nicastro, L., Feroci, M., Costa, E., Piro, L., Peterson, B. A., Tinney, C., Boyle, B., Cannon, R., Stathakis, R., Sadler, E., Begam, M. C., & Ianna, P. 1998b, Nature, 395, 670
 Garnavich, P., Jha, S., Kirshner, R., & Challis, P. 1997, IAU Circ. No. 6798
 Germany, L.M., Reiss, D.J., Schmidt, B.P., Stubbs, C.W., Sadler, E.M. 2000, ApJ, 533, 320
 Hachisu, I., Matsuda, T., Nomoto, K., & Shigeyama, T. 1991, ApJ, 368, 27
 Heger, A., Woosley, S. E., Waters, R. 2000, in The First Stars (ESO Astrophysics Symposia), eds. A. Weiss, T. Abel, & V. Hill (Berlin: Springer), 121
 Hix, W. R. & Thielemann, F.-K. 1996, ApJ, 460, 869
 Holland, S., Fynbo, J., Thomsen, B., Andersen, M., Bjornsson, G., Hjorth, J., Jaunsen, A., Natarajan, P., & Tanvir, N. 2000, GCN Cir. No.704
 Iwamoto, K., Nomoto, K., Höflich, P., Yamaoka, H., Kumagai, S., & Shigeyama, T. 1994, ApJ, 437, 115
 Iwamoto, K., Young, T.R., Nakasato, N., Shigeyama, T., Nomoto, K., Hachisu, I., Saio, H. 1997, ApJ, 477, 865
 Iwamoto, K., Mazzali, P. A., Nomoto, K., Umeda, H., Nakamura, T., Patat, F., Danziger, I. J., Young, T. R., Suzuki, T., Shigeyama, T., Augusteijn, T., Doublier, V., Gonzalez, J.-F., Boe hnhardt, H., Brewer, J., Hainaut, O.R., Lidman, C., Leibundgut, B., Cappellaro, E., Turatto, M., Galama, T. J., Vreeswijk, P. M., Kouveliotou, C., Paradijs, J.van, Pian, E., Palazzi, E., & Frontera F. 1998, Nature, 395, 672
 Iwamoto, K., Nakamura, T., Nomoto, K., Mazzali, P. A., Garnavich, P., Kirshner, R., Jha, S., Balam, D. & Thorsternsen, J. 2000, ApJ, 534, 660
 Khokhlov, A. M., Höflich, P. A., Oran, E. S., Wheeler, J. C., Wang, L., & Chtchelkanova, A. Yu. 1999, ApJ, 524, L107
 Kulkarni, S. R., Bloom, J. S., Frail, D. A., Ekers, R., Wieringa, M., Wark, R., & Higdon, J. L. 1998a, IAU Circ. No. 6903
 Kulkarni, S. R., Frail, D. A., Wieringa, M. H., Ekers, R. D., Sadler, E. M., Wark, R. M., Higdon, J. L., Phinney E. S., & Bloom, J. S. 1998b, Nature, 395, 663
 Lucy, L.B. 1999, A&A, 345, 211
 MacFadyen, A.I. & Woosley, S.E. 1999, ApJ, 524, 262
 Maeda, K., Nakamura, T., Nomoto, K., Mazzali, P. A., & Hachisu, I. 2000, in Origin of Matter and Evolution of Galaxies, ed. T. Kajino et al. (Singapore: World Scientific), in press
 Mazzali, P.A., & Lucy, L.B. 1993, A&A, 279, 447
 Mazzali, P.A. 2000, A&A, in press
 Mazzali, P.A., Iwamoto, K., & Nomoto, K. 2000a, ApJ, submitted
 Mazzali, P.A. et al. 2000b, in preparation
 McKenzie, E.H., & Schaefer, B.E. 1999, PASP, 111, 964
 Nagataki, S., Hashimoto, M., Sato, K., & Yamada, S. 1997, ApJ, 486, 1026
 Nakamura, T. 1998, Prog. Theor. Phys., 100, 921
 Nakamura, T., Mazzali, P.A., Nomoto, K., Iwamoto, K., & Umeda, H. 1999a, Astron. Nachrichten, 320, 363
 Nakamura, T., Umeda, H., Nomoto, K., Thielemann,F.-K., & Burrows,A. 1999b, ApJ, 517, 193
 Nakamura, T., Maeda, K., Iwamoto, K., Suzuki, T., Nomoto, K., Mazzali, P.A., Turatto, M., Danziger, I.J., & Patat, N. 2000, in IAU Symp. 195, Highly Energetic Physical Processes and Mechanisms for Emission from Astrophysical Plasmas, eds. P. Martens, S. Tsuruta, & M. Weber (PASP), 347
 Nakatsuru, J., Nakamura, T., Umeda, H., & Nomoto, K. 2000, in Origin of Matter and Evolution of Galaxies, ed. T. Kajino et al. (Singapore: World Scientific), in press
 Nomoto, K., Yamaoka, H., Pols, O.R., Van den Heuvel, E.P.J., Iwamoto, K., Kumagai, S., Shigeyama, T. 1994, Nature, 371, 227
 Nomoto, K., Hashimoto, M., Tsujimoto, T., Thielemann, F.-K., Kishimoto, N., Kubo, Y., & Nakasato, N. 1997, Nuclear Phys., A616, 79c
 Nomoto, K., Mazzali, P.A., Nakamura, T., Iwamoto, K., Maeda, K., Suzuki, T., Turatto, M., Danziger, I.J., & Patat, F. 2000a, in "Supernovae and Gamma Ray Bursts", ed. M. Livio et al. (Cambridge: Cambridge University Press), in press
 Nomoto, K., Maeda, K., Nakamura, T., Iwamoto, K., Suzuki, T., Mazzali, P.A., Turatto, M., Danziger, I.J., & Patat, F. 2000b, in Gamma Ray Bursts, ed. R. M. Kippen et al. (New York: AIP), in press
 Paczyński, B. 1998, ApJ, 494, 45
 Patat, F., & Piemonte, A. 1998, IAU Circ. No. 6918
 Patat, F. et al., 2000, ApJ, submitted
 Pian, E., Amati, L., Antonelli, L. A., Butler, R. C., Costa, E., Cusumano, G., Danziger, J., Feroci, M., Fiore, F., Frontera, F., Giommi, P., Masetti, N., Muller, J. M., Oosterbroek, T., Owens, A., Palazzi, E., Piro, L., Castro-Tirado, A., Coletta, A., dal Fiume, D., del Sordo, S., Heise, J., Nicastro, L., Orlandini, M., Parmar, A., Soffitta, P., Torroni, V., In't Zand, J. J. M. 1999, A&AS, 138, 463
 Piran, T. 1999, Physics Reports, 314, 575
 Richmond, M. W., et al. 1996a, AJ, 111, 327
 Richmond, M. W., Treffers, T. R., Filippenko, A. V., & Paik, Y. 1996b, AJ, 111, 732
 Soffitta, P., Feroci, M., & Piro, L. 1998, IAU Circ. No. 6884
 Stathakis, R.A., et al. 2000, MNRAS, submitted (astro-ph/0001497)
 Thielemann, F.-K., Nomoto, K., & Hashimoto, M. 1996, ApJ, 460, 408
 Turatto, M., Suzuki, T., Mazzali, P.A., Benetti, S., Cappellaro, E., Nomoto, K., Nakamura, T., Young, T.R., Patat, F. 2000, ApJ, 534, L57
 Wang, L., & Wheeler, J. C. 1998, ApJ, 504, L87
 Wang, L., Howell, A., Höflich, P. A., & Wheeler, J. C. 1999, ApJ, submitted (astro-ph/9912033)
 Wheeler, J. C., Yi, I., Höflich, P. A., & Wang, L. 2000, ApJ, in press
 Woosley, S. E. 1993, ApJ, 405, 273
 Woosley, S. E., Eastman, R. G., & Schmidt, B.P. 1999, ApJ, 516, 788

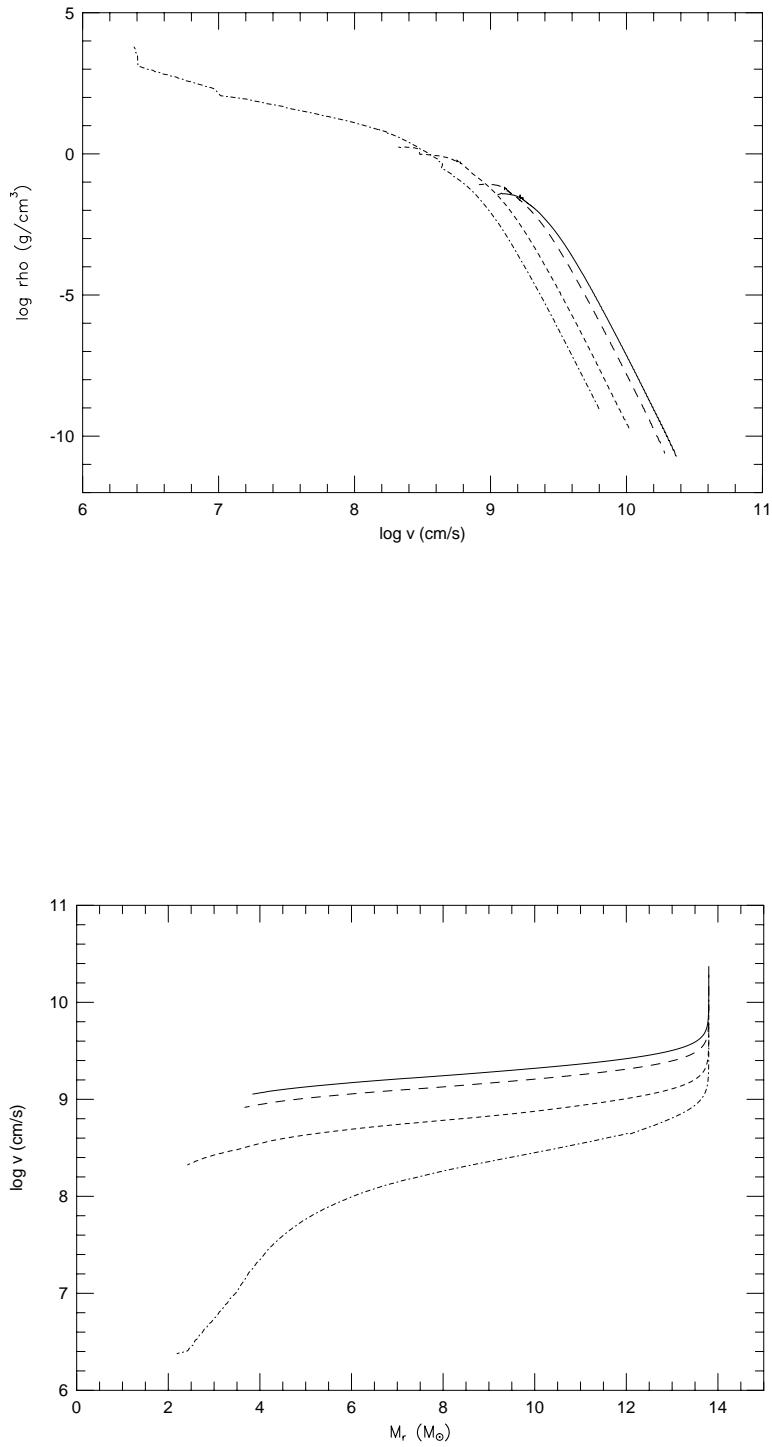


FIG. 1.— Density distributions against the velocity of homologously expanding ejecta (above) and the velocity profiles against the enclosed mass (below) for CO138E50 (solid line), CO138E30 (long-dashed line), CO138E7 (short-dashed line), and CO138E1 (dash-dotted line) at $t = 250$ sec.

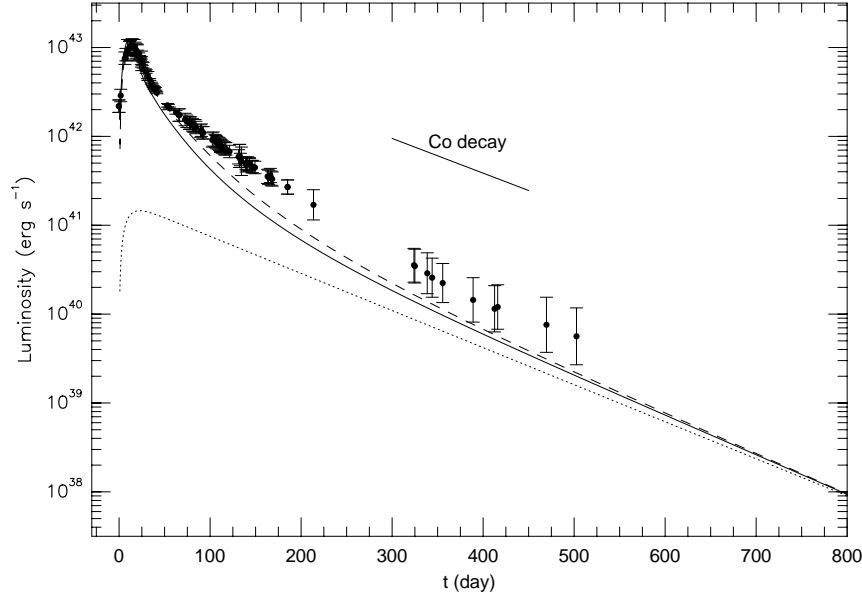


FIG. 2.— The light curves of CO138E50 ($E_K = 5 \times 10^{52}$ erg; solid line) and CO138E30 ($E_K = 3 \times 10^{52}$ erg; long-dashed line) compared with the bolometric light curve of SN1998bw (Patat et al. 2000). A distance modulus of $\mu = 32.89$ mag and $A_V = 0.05$ are adopted. The dotted line indicates the energy deposited by positrons for CO138E50.

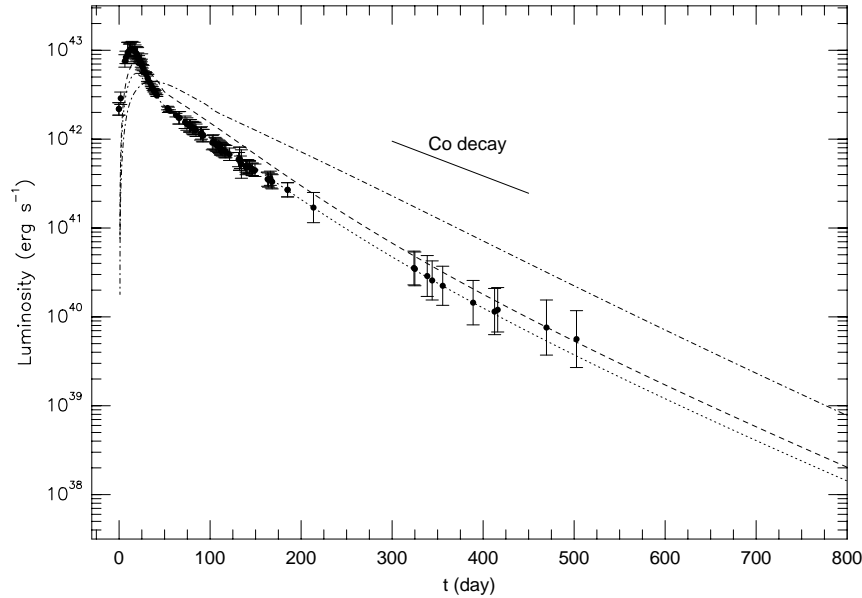


FIG. 3.— The light curves of CO138E7 ($E_K = 7 \times 10^{51}$ erg; dashed line) and CO138E1 ($E_K = 1 \times 10^{51}$ erg; dash-dotted line) compared with the bolometric light curve of SN1998bw (Patat et al. 2000). Also shown is the light curve of modified CO138E7 with smaller ^{56}Ni mass of $0.28M_\odot$ (dotted line).

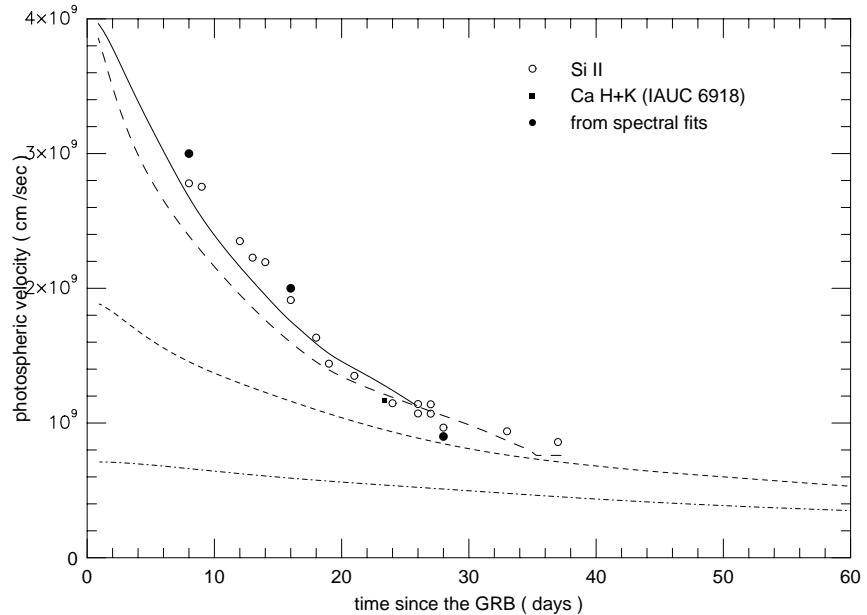


FIG. 4.— Photospheric velocities of CO138E50 (solid line), CO138E30 (long-dashed line), CO138E7 (short-dashed line), and CO138E1 (dash-dotted line) compared with the observations of SN1998bw. Shown are the photospheric velocities obtained from spectral models (filled circles, this paper), the observed velocity of the Si II 634.7, 637.1 nm lines measured in the spectra at the absorption core (open circles; Patat et al. 2000), and that of the Ca II H + K doublet measured in the spectrum of May 23 (square; Patat & Piemonte 1998).

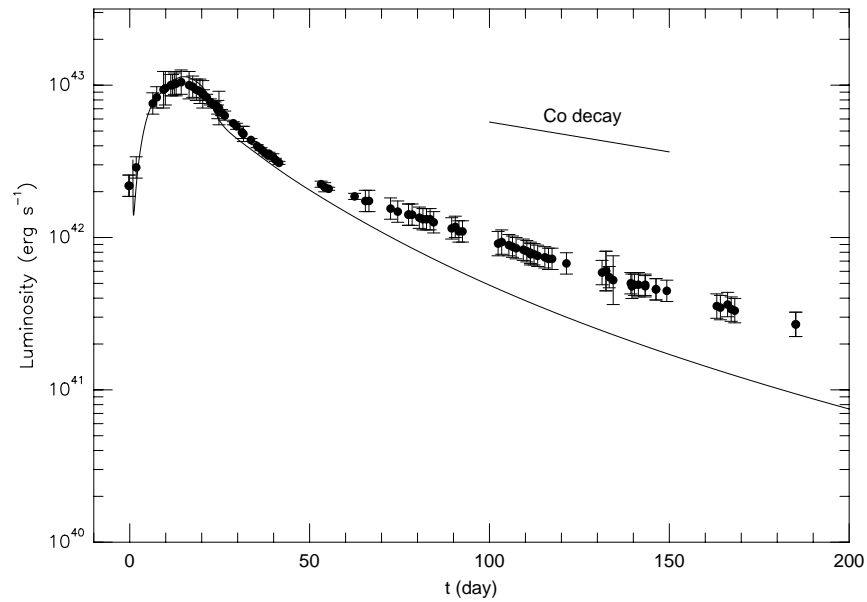


FIG. 5.— The early light curves of model CO138E50 with modified ^{56}Ni distribution (see text) compared with the bolometric light curve of SN1998bw (Patat et al. 2000).

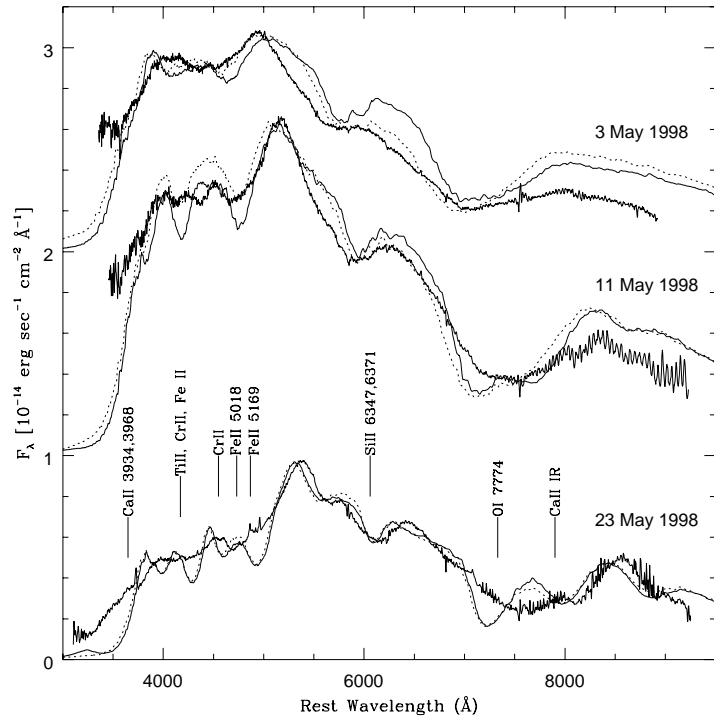
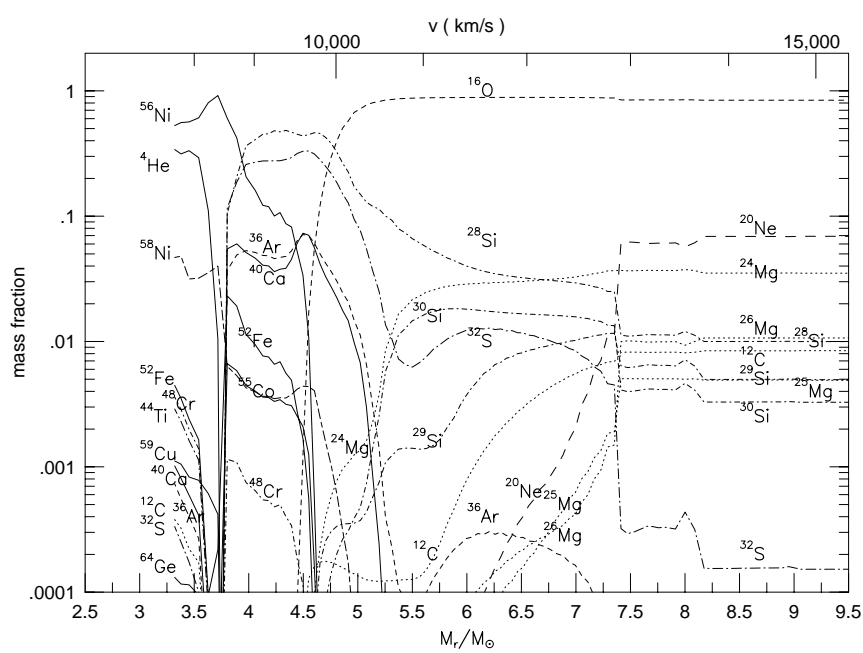
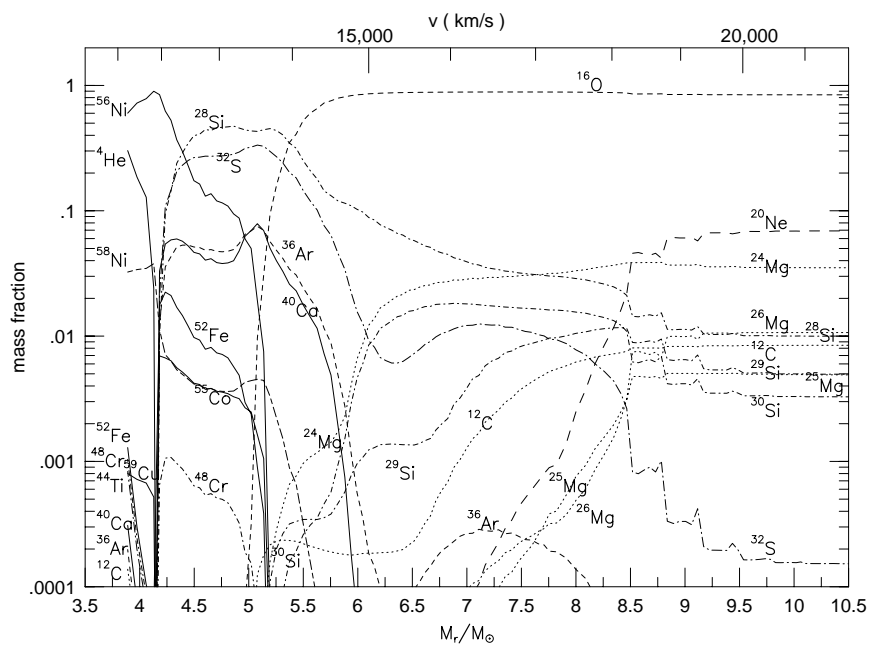


FIG. 6.— Three ESO spectra of SN 1998bw near maximum (bold lines) are compared with synthetic spectra obtained using model CO138E50 (continuous lines) and with spectra obtained for a modified density distribution as described in the text (dotted lines).



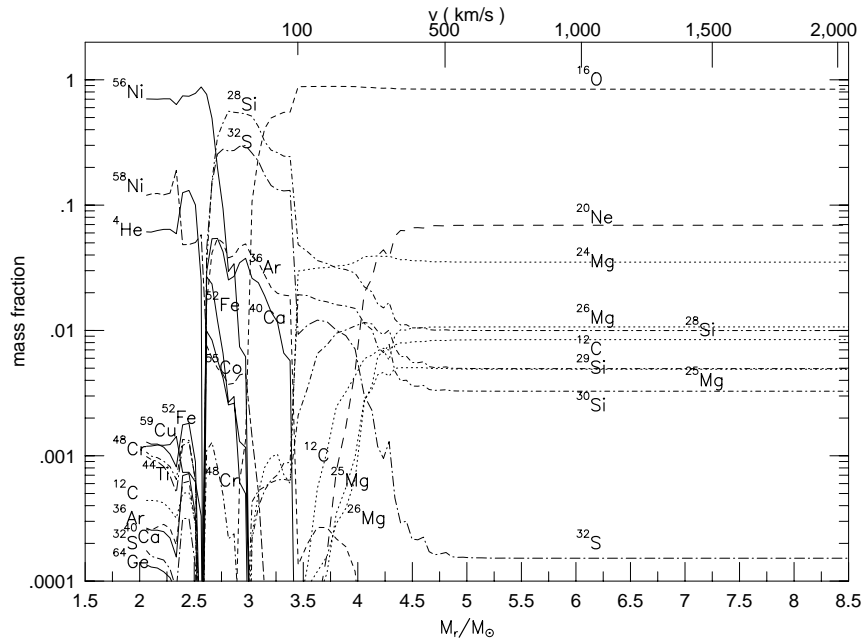
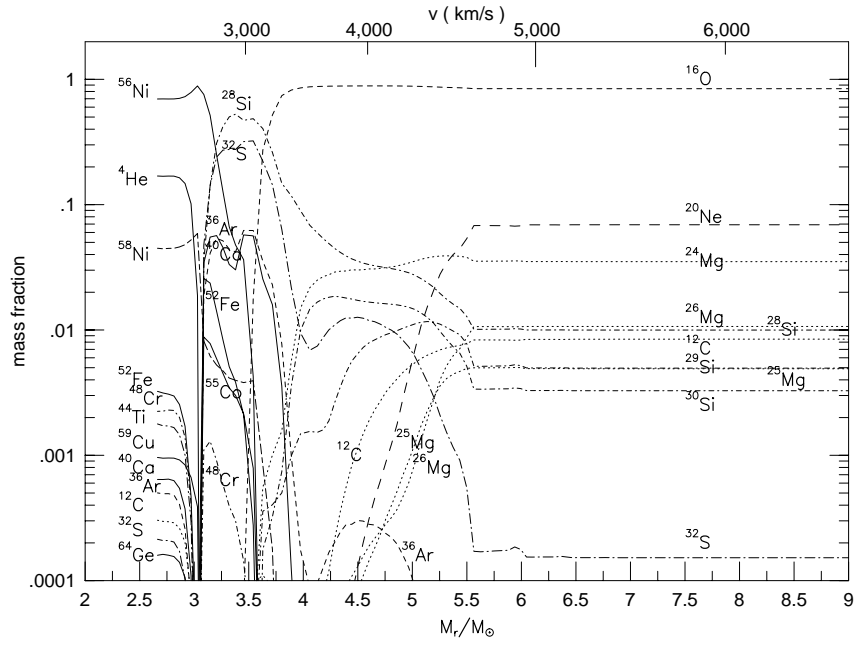


FIG. 7.— The isotopic composition of ejecta of hypernovae ($E_K = 5 \times 10^{52}$ ergs; top left), ($E_K = 3 \times 10^{52}$ ergs; top right), ($E_K = 7 \times 10^{51}$ ergs; bottom left), and usual supernovae ($E_K = 1 \times 10^{51}$ erg; bottom right). Only the dominant species are plotted. The explosive nucleosynthesis is calculated using a detailed nuclear reaction network including a total of 211 isotopes up to ^{71}Ge .

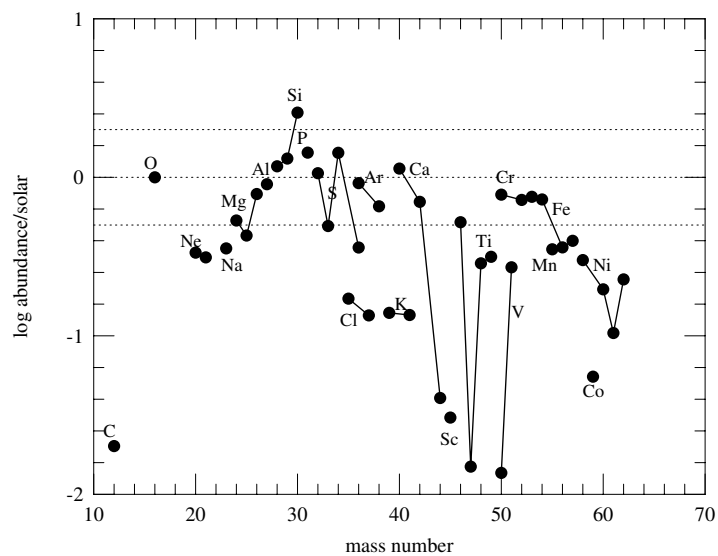


FIG. 8.— Abundances of stable isotopes relative to the solar values for model CO138E50.

model	$M_{\text{ms}}(M_{\odot})$	$M_{\text{C+O}}$	M_{ej}	^{56}Ni mass	M_{cut}	$E_{\text{K}} (10^{51} \text{ erg})$
CO138E1	~ 40	13.8	12	0.4	2	1
CO138E7	~ 40	13.8	11.5	0.4	2.5	7
CO138E30	~ 40	13.8	10.5	0.4	3.5	30
CO138E50	~ 40	13.8	10	0.4	4	50

TABLE 1
PARAMETERS OF THE C+O STAR MODELS.

model	C	O	Ne	Mg	Si	S	Ca	Ti	Fe	Ni
CO138E1	0.10	8.9	0.66	0.51	0.52	0.19	0.023	0.0007	0.44	0.065
CO138E7	0.09	8.5	0.58	0.47	0.52	0.19	0.029	0.0010	0.44	0.036
CO138E30	0.07	7.6	0.44	0.38	0.74	0.35	0.054	0.0009	0.45	0.023
CO138E50	0.06	7.1	0.37	0.34	0.83	0.41	0.066	0.0007	0.46	0.018

model	^{44}Ti	^{56}Ni	^{57}Ni
CO138E1	3.4×10^{-4}	0.40	1.6×10^{-2}
CO138E7	4.5×10^{-4}	0.40	1.4×10^{-2}
CO138E30	2.3×10^{-4}	0.40	1.2×10^{-2}
CO138E50	5.5×10^{-5}	0.40	1.1×10^{-2}

TABLE 2
YIELDS OF HYPERNOVA AND SUPERNOVA MODELS (M_{\odot}).

^{12}C	6.45E-02	^{13}C	2.57E-08	^{14}N	1.34E-07	^{15}N	4.08E-08	^{16}O	7.07
^{17}O	1.76E-07	^{18}O	2.45E-08	^{19}F	1.12E-08	^{20}Ne	3.72E-01	^{21}Ne	1.10E-03
^{22}Ne	5.49E-04	^{23}Na	1.18E-02	^{24}Mg	2.57E-01	^{25}Mg	2.76E-02	^{26}Mg	5.78E-02
^{27}Al	4.99E-02	^{28}Si	7.27E-01	^{29}Si	4.30E-02	^{30}Si	5.70E-02	^{31}P	6.93E-03
^{32}S	3.88E-01	^{33}S	1.48E-03	^{34}S	2.46E-02	^{36}S	2.12E-05	^{35}Cl	5.17E-04
^{37}Cl	1.39E-04	^{36}Ar	7.10E-02	^{38}Ar	1.00E-02	^{40}Ar	2.85E-07	^{39}K	4.26E-04
^{41}K	3.21E-05	^{40}Ca	6.61E-02	^{42}Ca	2.83E-04	^{43}Ca	4.60E-07	^{44}Ca	5.53E-05
^{46}Ca	5.53E-10	^{48}Ca	7.90E-14	^{45}Sc	1.02E-06	^{46}Ti	1.09E-04	^{47}Ti	2.96E-06
^{48}Ti	5.87E-04	^{49}Ti	4.90E-05	^{50}Ti	4.15E-09	^{50}V	1.00E-08	^{51}V	8.39E-05
^{50}Cr	5.11E-04	^{52}Cr	9.53E-03	^{53}Cr	1.16E-03	^{54}Cr	3.07E-07	^{55}Mn	4.32E-03
^{54}Fe	4.92E-02	^{56}Fe	4.01E-01	^{57}Fe	1.07E-02	^{58}Fe	1.04E-07	^{59}Co	1.72E-04
^{58}Ni	1.36E-02	^{60}Ni	3.54E-03	^{61}Ni	8.69E-05	^{62}Ni	5.91E-04	^{64}Ni	3.10E-13
^{63}Cu	3.47E-07	^{65}Cu	2.36E-07	^{64}Zn	6.49E-06	^{66}Zn	3.91E-06	^{67}Zn	3.03E-09
^{68}Zn	1.93E-09								

TABLE 3
DETAILED YIELDS OF MODEL CO138E50 (M_{\odot}).